RESEARCH DEPARTMENT

The determination of dipole reactance by radiation pattern integration

RESEARCH REPORT No. RA-1

UDC 621. 396. 677: 621. 3. 095. 4. 1967/5

THE BRITISH BROADCASTING CORPORATION
ENGINEERING DIVISION

RESEARCH DEPARTMENT

THE DETERMINATION OF DIPOLE REACTANCE BY RADIATION PATTERN INTEGRATION

Research Report No. RA-1
UDC 621.396.677 1967/5
621.3.095.4

P.C.J. Hill, Ph.D., B.Sc., D.I.C.

Head of Research Department

Research Report No. RA-1

THE DETERMINATION OF DIPOLE REACTANCE BY RADIATION PATTERN INTEGRATION

February 1967

Research Report No. RA-1
UDC 621.396.677 1967/5
621.3.095.4

THE DETERMINATION OF DIPOLE REACTANCE BY RADIATION PATTERN INTEGRATION

SUMMARY

A new method for determining the input reactance of a cylindrical dipole is given based upon the principle of analytic continuation of Poynting integration into the part of the radiation pattern outside the normal, or 'visible' region. The theoretical basis for this extension, recently described by Rhodes[1] for the case of planar aerials, is re-stated here and then applied to cylindrical systems. The reactance of a thin dipole is evaluated for a range of dipole sizes and the results compared with those obtained by the well-known induced e.m.f. method.

LIST OF PRINCIPAL SYMBOLS

a dipole radius
d separation of current filaments
E electric intensity vector (volts/metre)
$F(\mu)$ Fourier transform of current distribution $I(z)$
H magnetic intensity vector (amps/metre)
$H_0^{(2)}(u)$, $H_1^{(2)}(u)$ Hankel functions of the 2nd kind, zero and first orders ($= J_{0,1}(u) - jY_{0,1}(u)$)
I filamentary current
I_0 dipole loop current
I_s uniform sheet current
$I(z)$ current distribution
J_z current line density (amps/metre)
k phase constant ($= 2\pi/\lambda$)
l dipole half-length
P power (watts)
$P(\alpha)$, $P(\beta)$ angular spectra
$p(\psi)$, $p(\mu)$ pattern functions
r, θ, ϕ spherical co-ordinate variables
R radiation resistance (ohms)
u parameter defined by $u = ka(1 - \mu^2)^{\frac{1}{2}}$
v parameter defined by $v = ka(\mu^2 - 1)^{\frac{1}{2}}$
W strip width
x, y, z cartesian co-ordinate variables
X input reactance (ohms)
Z total input impedance ($= R + jX$)
Z_M, Z_S mutual and self-impedances
α, β angular spectrum variables
$\delta(y)$ Dirac delta function
$\log \gamma$ Euler's constant ($= 0{\cdot}5772\ldots$)
η_0 wave impedance of free space (120π ohms)
λ wavelength
μ pattern function variable ($= \sin \alpha$)
ρ, ϕ, z cylindrical co-ordinate variables
ψ pattern function variable ($= \sin \beta$)
$\underline{\psi}$ scalar potential function

1. INTRODUCTION

There are two well-known methods for determining the radiation resistance of an aerial. In the 'Poynting vector method', integration of the far-field power pattern over all real angles gives the real (resistive) power radiated by the aerial. In the 'induced-e.m.f. method', integration of the power flux over a surface tightly fitting the radiating elements of the aerial gives the complex radiated power; the real part is identical to that given by the Poynting method whereas the imaginary part corresponds to the power stored in the so-called induction field of the aerial and this determines the input reactance. Since the Poynting vector method uses the far-field expressions for pattern integration it has always been assumed that it cannot be employed to determine aerial reactance. In a recent paper by Rhodes, however, it was shown that by extending the range of integration into a complex angular region, the method will give both the radiation resistance and the input reactance of a planar

aerial. The theoretical basis for this extension of the classical Poynting vector method to the complex angular region, or 'invisible' part of the radiation pattern, had been set out previously in a most elegant paper by Woodward and Lawson[2]. Their starting point was the plane-wave integral representation[3] of electromagnetic fields existing on one side of a plane aperture. It was shown that, for transverse-magnetic (TM) fields in two dimensions, the far-field radiation pattern is identical to the 'angular spectrum' of plane-waves in the visible region (i.e. corresponding to the range of real angles). It was also shown that the radiation pattern and the fields at the aperture are related through the Fourier transform, and finally, that the radiation pattern lying outside the visible region determines the reactive power stored in the vicinity of the aperture.

In Reference 1, these results were extended to the general case in which the total fields of a linear, time-invariant, planar aerial are represented by a combination of TE - and TM - fields. The analysis was taken one step further by integrating the Poynting vector over the visible and invisible parts of the radiation pattern to determine the input impedance of a planar aerial.

The main purpose of this report is to extend the new principle to cylindrical systems and, in particular, to employ it for determining the reactance of a cylindrical dipole. As the method is not widely known, the report commences with a tutorial introduction to the basic principles involved.

2. BASIC PRINCIPLES

The theoretical basis for the extension of the classical Poynting vector method to the invisible part of the radiation pattern is most easily demonstrated for the case of planar aerials; the key to the method is the concept of an angular spectrum of waves and its identity with the far-field radiation pattern.

2.1. Angular Spectrum and Radiation Pattern

Following Woodward and Lawson[2], we consider the two-dimensional system shown in Fig. 1 in which OYZ is the aperture plane with waves being propagated only into the half-space given by $x > 0$. There is no field variation in the z-direction and the electric field E is chosen to be everywhere parallel to OZ; symmetry between E and H enables $\eta_0 H$ to be interchanged with E throughout, where η_0 is the wave-impedance of free-space.

An infinite plane-wave directed at an angle β to OX, with magnitude $P(\beta)\, d\beta$ referred to the origin, O, is fully specified by the expression:

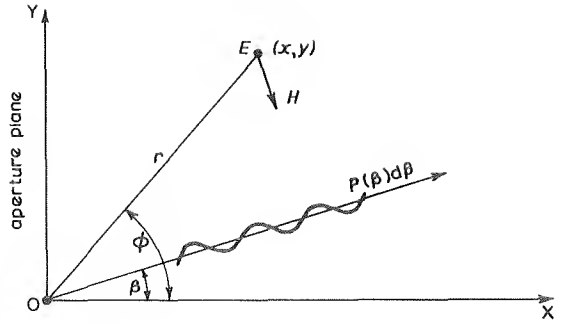

Fig. 1 - Angular spectrum of plane waves

$$P(\beta)\, d\beta\, e^{-jk(x\cos\beta + y\sin\beta)}$$

in which $k = 2\pi/\lambda$ with λ the free-space wavelength; the time-factor $e^{j\omega t}$ has been suppressed*. The function $P(\beta)$ represents the angular spectrum of a set of infinite plane-waves and is a complex quantity. In general, the fields at a point (x, y) will be due to a combination of such waves so that we have:

$$E_z(x,y) = \int_C P(\beta)\, e^{-jk(x\cos\beta + y\sin\beta)}\, d\beta \qquad (1)$$

The magnetic intensities $H_x(x,y)$ and $H_y(x,y)$ are given by expressions similar to Equation (1) through the relations $\eta_0\, dH_x = \sin\beta\, dE_z$ and $\eta_0\, dH_y = -\cos\beta\, dE_z$; these expressions are:

$$H_x(x,y) = \frac{1}{\eta_0} \int_C P(\beta)\, e^{-jk(x\cos\beta + y\sin\beta)} \sin\beta\, d\beta \qquad (2)$$

and:

$$H_y(x,y) = -\frac{1}{\eta_0} \int_C P(\beta)\, e^{-jk(x\cos\beta + y\sin\beta)} \cos\beta\, d\beta \qquad (3)$$

The remaining fields are given by $E_x = E_y = H_z = 0$.

In the above equations, the contour of integration C in the β-plane must be carefully selected; it must be such that, for positive x and for positive and negative y, the exponential term does not tend to infinity at any point along it. We may therefore admit complex values of β ($= \beta_R + j\beta_I$) provided that $\cos\beta$ is given no positive imaginary part and that $\sin\beta$ remains purely real. It follows from these conditions that the signs of β_R and β_I must be

* Since the time-factor is $e^{+j\omega t}$ a positive travelling wave is given by e^{-jkR}; in Reference 3, the negative exponent is used for the time-factor.

identical ($|\beta_R| \leq \pi$) and that β_I may not be non-zero unless $\beta_R = \pm \frac{\pi}{2}$. The resultant contour of integration is shown in Fig. 2(a); path C_2 is over the range of real angles (visible pattern region) and paths C_1, C_3 are over the allowed range of complex angles (invisible pattern region).

Equations (1), (2) and (3) give the field conditions at any point in the region to the right of the aperture (x positive) including the aperture plane itself ($x = 0$). By evaluating the field quantities at a great distance from the aperture we can show that the angular spectrum $P(\beta)$ is just the far-field complex radiation pattern of the source. Selecting $E_z(x,y)$ and referring to Fig. 1 we can re-write Equation (1) as:

$$E_z(r,\phi) = \int_C P(\beta) e^{-jkr\cos(\phi - \beta)}\, d\beta \qquad (4)$$

where r is the radial distance from the origin O. For large r, this integral may be evaluated by the method of stationary phase[4], since the integrand makes a significant contribution only near the region $\beta = \phi$; moreover, the contour paths C_1, C_3 are excluded from the range of integration since the integrand is greatly attenuated in the invisible region with r large. Near $\beta = \phi$, we may replace $P(\beta)$ with $P(\phi)$ and expand $\cos(\phi - \beta)$ into $1 - (\phi - \beta)^2/2$; Equation (4) then becomes:

$$E_z(r,\phi) \underset{r\to\infty}{\simeq} P(\phi) e^{-jkr} \int_{-\pi/2}^{\pi/2} e^{j\frac{kr}{2}(\phi - \beta)^2} d\beta$$

The limits of integration may be extended to $\pm\infty$ without invalidating the result because of the highly oscillatory nature of the integrand. Evaluation of the resulting standard integral gives:

$$E_z(r,\phi) \underset{r\to\infty}{\simeq} \frac{P(\phi)}{(r/\lambda)^{1/2}} e^{\,j(\frac{\pi}{4} - kr)} \qquad (5)$$

which identifies $P(\phi)$ as the far-field radiation pattern of the two-dimensional source. With a three-dimensional system, the above method yields the familiar r^{-1} dependence for the far-field of a point source[1].

2.2. Fourier Relationships

The fields existing at the aperture plane (Fig. 1) are given by Equations (1), (2) and (3) with $x = 0$; i.e. the tangential electric intensity is given by:

$$E_z(y) = \int_C P(\beta) e^{-jky\sin\beta} d\beta \qquad (6)$$

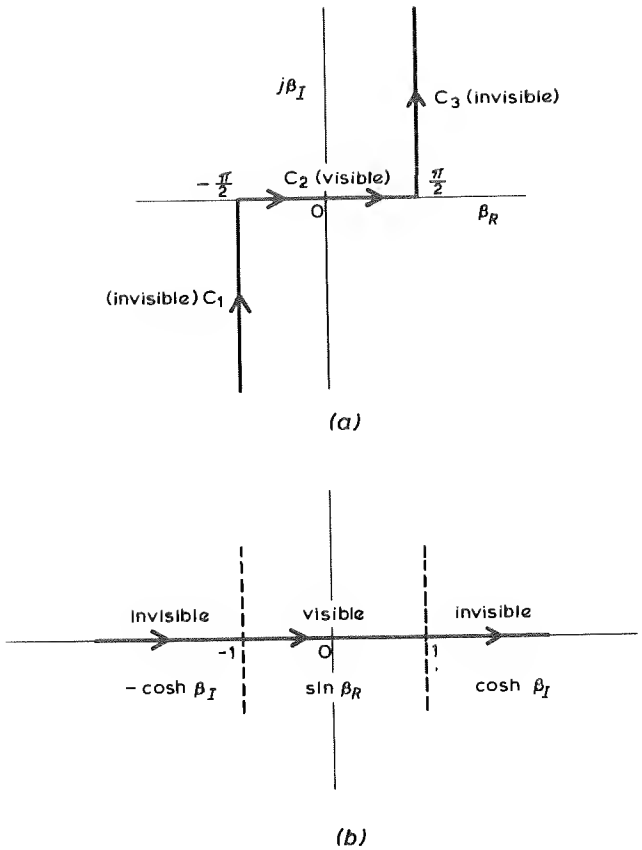

Fig. 2 - Contours of integration
(*a*) β-plane (*b*) ψ-plane

and replacing $P(\beta)$ by $-\frac{1}{\eta_0} P(\beta)\cos\beta$ in this equation gives $H_y(y)$. It is convenient to introduce a new variable ψ defined by:

$$\psi = \sin\beta \qquad (7)$$

so that the path of integration in the β-plane (Fig. 2(a)) becomes the real axis in the ψ-plane (Fig. 2 (b)). Equation (6) can now be written as:

$$E_z(y) = \int_{-\infty}^{\infty} \frac{p(\psi)}{(1-\psi^2)^{1/2}} e^{-jky\psi} d\psi \qquad (8)$$

in which $p(\psi)$ ($=P(\beta)$) is a new pattern function (the angular spectrum expressed as a function of $\sin\beta$); the visible region now corresponds to $-1 < \psi < 1$ and the invisible region lies outside this range, i.e. $|\psi| > 1$. We can now invert the relationship between $E_z(y)$ and $p(\psi)$ in Equation (8) by the Fourier transform theorem, viz.

$$p(\psi) = \frac{k(1-\psi^2)^{1/2}}{2\pi} \int_{-\infty}^{\infty} E_z(y) e^{jky\psi} dy \qquad (9)$$

Equations (8) and (9) are the connecting relations between the far-field pattern function $p(\psi)$ and the tangential electric intensity $E_z(y)$ in the aperture. Starting from Equation (3), it can be shown that the corresponding pair of equations involving the tangential magnetic intensity in the aperture are:

$$H_y(y) = -\frac{1}{\eta_0}\int_{-\infty}^{\infty} p(\psi)e^{-jky\psi}\,d\psi \qquad (10)$$

and

$$p(\psi) = -\frac{k\eta_0}{2\pi}\int_{-\infty}^{\infty} H_y(y)e^{jky\psi}\,dy \qquad (11)$$

The magnetic intensity $H_y(y)$ is identical to $J_z(y)$, where $J_z(y)$ is the current density in a plane aerial*, which is also independent of z. Bearing in mind that, in practice, the width of the aperture in the y-direction would be finite we see that Equation (10) can be used as the basis for synthesis of a continuous linear source from a given pattern function.

We are now in a position to discuss the significance of the visible and invisible parts of the radiation pattern function.

2.3. Poynting Integration with Complex Angles

From Poynting's theorem, the mean power flux density through any point in the aperture (Fig. 1) in the positive x-direction is the product of $-E_z(y)$ and $\overline{H_y(y)}$**; hence the mean power P through each infinite aperture strip of unit height (in the z-direction) is:

$$P = -\int_{-\infty}^{\infty} E_z(y)\overline{H_y(y)}\,dy$$

Substituting the expressions for $E_z(y)$ and $H_y(y)$ from Equations (8) and (10) we have:

$$P = \frac{1}{\eta_0}\int_{-\infty}^{\infty}\left(\int_{-\infty}^{\infty}\frac{p(\psi)e^{-jky\psi}}{(1-\psi^2)^{1/2}}\,d\psi\right)\left(\int_{-\infty}^{\infty}\overline{p(\psi)}e^{jky\psi}d\psi\right)dy$$

We can now apply the convolution theorem[5] in order to invert the product of the transforms within the brackets obtaining an integral expression for P in terms of the pattern function $p(\psi)$ (see Appendix, Section 7):

$$P = \frac{2\pi}{k\eta_0}\int_{-\infty}^{\infty}\frac{|p(\psi)|^2}{(1-\psi^2)^{1/2}}\,d\psi \qquad (12)$$

The factor 2π has appeared in this equation because we have employed the asymmetrical transform (Section 2.2). Equation (12) gives the mean complex power flowing through each unit strip of the aperture; the real part Re(P) is the resistive (radiated) power and the imaginary part Im(P) is the reactive power, both quantities being expressed in terms of the far-field power pattern $|p(\psi)|^2$. Because $(1-\psi^2)^{1/2}$ is real for $-1<\psi<1$ and imaginary outside this range, it follows that Re(P) is obtained by restricting the pattern integration to the visible region, $-1<\psi<1$, (the conventional Poynting vector method), and also that Im(P) is obtained by allowing the integration to extend over the invisible region, $|\psi|>1$, where the denominator of the weighted power pattern, $(1-\psi^2)^{1/2}$, becomes $-j(\psi^2-1)^{1/2}$ i.e.

$$\mathrm{Re}(P) = \frac{2\pi}{k\eta_0}\int_{-1}^{1}\frac{|p(\psi)|^2}{(1-\psi^2)^{1/2}}\,d\psi$$

$$\mathrm{Im}(P) = \frac{2\pi}{k\eta_0}\left[\int_{-\infty}^{-1} + \int_{1}^{\infty}\right]\frac{|p(\psi)|^2}{(\psi^2-1)^{1/2}}\,d\psi \qquad (13)^*$$

Once the pattern function $|p(\psi)|$ of the strip is known, Equations (13) give the radiation resistance R and the input reactance X through the relations, Re(P) = I_s^2R and Im(P) = I_s^2X where I_s is the current at the input terminals of the aerial occupying the aperture. Equations (13) can be combined into a single expression for the total input impedance $Z(= R + jX)$ by writing

$$Z = \frac{2\pi}{k\eta_0 I_s^2}\int_{-\infty}^{\infty}\frac{|p(\psi)|^2}{(1-\psi^2)^{1/2}}\,d\psi \qquad (14)$$

In using Equation (14) we recall that the denominator of the integrand becomes $-j(\psi^2-1)^{1/2}$ in the invisible region, $|\psi|>1$.

2.4. Illustrative Examples

Let us consider an aperture which is uniformly illuminated over a total width W (Fig. 3(a)), then we have $I_s/W = J_z(y) = H_y(y)$. In order to evaluate R

* We are only concerned here with the current which flows on one side of the "sheet".

** The superior bar denotes the complex conjugate.

* "Re" and "Im" denote the "real" and "imaginary part of" respectively.

and X it is first necessary to obtain $p(\psi)$ through the transform relation given in Equation (11) by substituting $H_y(y) = I_S/W$. The rectangular current distribution transforms into a "sinc" pattern function* giving,

$$p(\psi) = \frac{-\eta_0 I_S}{\pi} \frac{\sin(kW\psi/2)}{W\psi}$$

The power pattern, $|p(\psi)|^2$, illustrated in Fig. 3 (b), can now be inserted into Equation (14) which yields the following integral expressions for R and X:

$$R = \frac{4\eta_0}{\pi k W^2} \int_0^1 \frac{\sin^2(kW\psi/2)}{\psi^2(1-\psi^2)^{1/2}} d\psi$$

$$X = \frac{4\eta_0}{\pi k W^2} \int_1^\infty \frac{\sin^2(kW\psi/2)}{\psi^2(\psi^2-1)^{1/2}} d\psi$$

The above integrals, although quite formidable for arbitrary W, become straightforward for the extreme cases of an infinitely narrow ($W \to 0$) and an infinitely wide strip ($W \to \infty$) where the sinc-squared pattern collapses into an omnidirectional and a delta-function pattern respectively. For example, in the first case with $W \to 0$, we find that $R = k\eta_0/2$ and $X = \infty$ so that a uniform filamentary aerial (radiating from both sides) has a radiation resistance $60\pi^2/\lambda$ ohms per unit length and infinite reactance; this result agrees with results obtained by conventional methods.

As a second example, we shall show how the same technique can be used to determine the mutual impedance between two parallel radiating infinite filamentary currents I spaced d apart; the previous results may be used directly if it is assumed initially that the filaments are plane and radiate from one side only. The magnetic intensity over the aperture may be written as,

$$H_y(y) = I\{\delta(y + d/2) + \delta(y - d/2)\}$$

where $\delta(y)$ is the Dirac delta function, and if this is substituted into Equation (11) we obtain the pattern function $p(\psi)$, i.e.

$$p(\psi) = -\frac{k\eta_0 I}{\pi} \cos\left(\frac{kd\psi}{2}\right)$$

* The sinc function is defined by the relation $\text{sinc } x = \frac{\sin \pi x}{\pi x}$

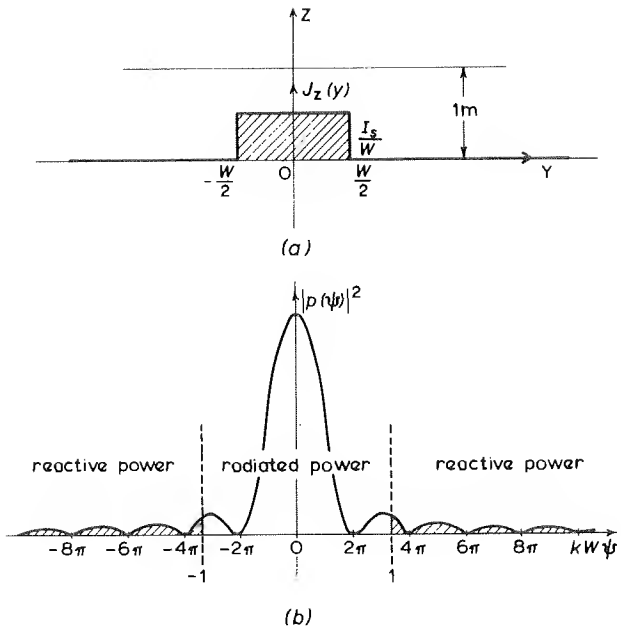

Fig. 3 - Uniform current sheet carrying total current I_S
(*a*) current distribution $J_z(y)$
(*b*) power pattern function $|p(\psi)|^2$

The total complex power radiated by the aperture is $2I^2(Z_S + Z_M)$ where Z_S and Z_M are the self-and mutual impedances of the filaments respectively. Equation (14) therefore gives an expression for $(Z_S + Z_M)$ on inserting $I_S^2 = 2I^2$ and $|p(\psi)|^2$ from the above relation, viz

$$Z_S + Z_M = \frac{2k\eta_0}{\pi} \int_0^\infty \frac{\cos^2(kd\psi/2)}{(1 - \psi^2)^{1/2}} d\psi$$

$$= \frac{k\eta_0}{\pi} \int_0^\infty \frac{1 + \cos(kd\psi)}{(1 - \psi^2)^{1/2}} d\psi$$

But we have already shown that for a current filament,

$$Z_S = \frac{k\eta_0}{\pi} \int_0^\infty \frac{d\psi}{(1-\psi^2)^{1/2}}$$

so it follows that

$$Z_M = \frac{k\eta_0}{\pi} \int_0^\infty \frac{\cos(kd\psi)}{(1-\psi^2)^{1/2}} d\psi$$

The latter integral is in standard form and gives

$$Z_M = \frac{k\eta_0}{2} H_0^{(2)}(kd)$$

where $H_0^{(2)}$ is the zero-order Hankel function of the second kind. We therefore have the result that the mutual impedance between two parallel current filaments (radiating from both sides) is:

$$\frac{60\pi^2}{\lambda} H_0^{(2)}(kd)$$

ohms per unit length which is in agreement with that obtained by conventional methods.

It has been demonstrated that the total impedance Z of a two-dimensional plane aerial can be obtained by Poynting integration of the far-field power pattern; the extension to the three-dimensional case is contained in Reference 1, where the resistance and reactance of a narrow planar dipole are evaluated by this method.

3. APPLICATION TO CYLINDRICAL AERIALS

The principles underlying the new method of determining the total impedance of a planar aerial from its radiation pattern were described in Section 2. We can now turn our attention to the problem of developing a similar method for evaluating the reactance of cylindrical aerials. In this case, our starting point will involve the concept of an angular spectrum of cylindrical waves. The discussion which follows will be limited to systems possessing axial symmetry.

3.1. Integral Relationships for Cylindrical Aerials

We shall consider the three-dimensional system shown in Fig. 4 in which a cylindrical aperture of radius a and with its axis directed along OZ radiates outward travelling cylindrical waves. An elementary TM-cylindrical wave with axial symmetry directed at an angle α to the horizontal with magnitude $P(\alpha)d\alpha$ referred to the origin O is fully specified by the following scalar potential function,

$$d\underline{\psi}(\rho,z) = P(\alpha)d\alpha\, H_0^{(2)}(k\rho\cos\alpha)e^{-jkz\sin\alpha}$$

where the time-factor $e^{j\omega t}$ has been suppressed. The elementary field components are then given through the expressions[6],

$$dE_z = k^2\cos^2\alpha\, d\underline{\psi}, \quad dH_\phi = -\frac{jk}{\eta_0}\frac{\partial}{\partial\rho}(d\underline{\psi})$$

$$dE_\rho = \pm\frac{jk\sin\alpha}{\rho}\frac{\partial}{\partial\rho}(d\psi), \quad dE_\phi = dH_\rho = dH_z = 0.$$

since there is no variation with ϕ. In general, the total field at a point (ρ,z) outside the aperture will be due to a combination of such waves so that we can write,

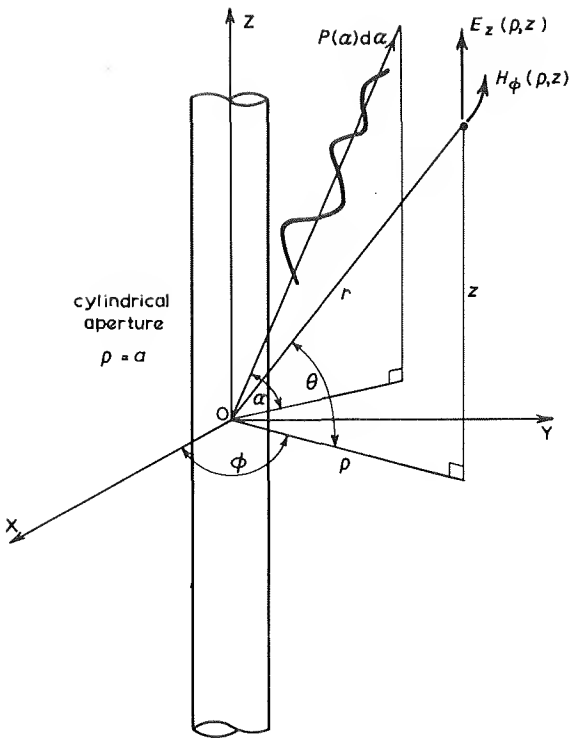

Fig. 4 - Angular spectrum of cylindrical waves with axial symmetry

$$E_z(\rho,z) = \int_C P(\alpha)k^2\cos^2\alpha H_0^{(2)}(k\rho\cos\alpha)e^{-jkz\sin\alpha}d\alpha \tag{15}$$

and

$$H_\phi(\rho,z) = \frac{jk}{\eta_0}\int_C P(\alpha)k\cos\alpha H_1^{(2)}(k\rho\cos\alpha)e^{-jkz\sin\alpha}d\alpha \tag{16}$$

Equations (15) and (16) can alternatively be derived directly from Maxwell's equations in cylindrical coordinates. As with the plane-wave case, symmetry between E and H enables $\eta_0 H$ to be interchanged with E throughout so that the following analysis also includes systems involving transverse-electric (TE) cylindrical waves.

The contour of integration C in the above integral expressions must be carefully chosen; the path must be such that for $\rho \geqslant a$ (positive) and $-\infty < z < \infty$ the cosine-Hankel-exponential functions in the integrands of Equations (15) and (16) remain finite over the path in the α-plane. The condition involving the exponential function is as before, namely complex values of $\alpha(=\alpha_R + j\alpha_I)$ are admitted provided that $\sin\alpha$ remains purely real, i.e. α_I must equal zero unless $\alpha_R = \pm\pi/2$; the conditions involving the Hankel functions are not so straightforward and will now be elaborated. The

functions $H^{(2)}_{0,1}(k\rho\cos\alpha)$ must not increase indefinitely as $\rho(\geq a)$ is increased towards infinity for values of α which, from the previous condition are given by

$$\alpha = \alpha_R \text{ and } \alpha = \pm\frac{\pi}{2} \pm j\alpha_I;$$

we need only consider, therefore, the argument $k\rho\cos\alpha$ in each of three states: finite real and positive, zero, and purely imaginary. The following properties of the Hankel function are relevant:

(i) $H^{(2)}_{0,1}(\nu)$ is complex unless ν is imaginary when $H^{(2)}_0(\nu)$ is imaginary but $H^{(2)}_1(\nu)$ is real.

(ii) For ν equal to zero, $|H^{(2)}_{0,1}(\nu)|$ becomes infinite.

(iii) The asymptotic formulae for large ν are valid for ν complex, i.e.

$$H^{(2)}_n(\nu) \simeq \left(\frac{2}{\pi\nu}\right)^{1/2} e^{-j(\nu - n\pi/2 - \pi/4)}$$

It follows that $\cos\alpha$ must not contain any positive imaginary part, i.e. the signs of α_R and α_I must be identical ($|\alpha_R| \leq \pi$); the poles in the Hankel functions which occur with $\alpha = \pm\pi/2$ appear in the scalar wave function ψ but in the expressions for E_z and H_ϕ (Equations (15) and (16) they are annihilated by the $\cos\alpha$ weighting functions. For the field quantities therefore, the resultant contour of integration in the α-plane is identical to that given previously for β in the plane-wave case (Fig. 2 (a)); as before, path C_2 is over real (visible) angles and paths C_1, C_3 are over complex (invisible) angles.

Evaluating the field quantities given by Equations (15) and (16) at a great distance from the aperture ($r \to \infty$) we can show that the angular spectrum $P(\alpha)$ is just the far-field complex radiation pattern of the source. Selecting $E_z(\rho,z)$ and referring to Fig. 4 we can re-write Equation (15) in a form suitable for stationary-phase integration (Section 2.1) by inserting $\rho = r\cos\theta$, $z = r\sin\theta$ and writing $H^{(2)}_0(k\rho\cos\alpha)$ in asymptotic form for large r. On performing the integration we obtain the result,

$$E_z(r,\theta) \underset{r\to\infty}{\simeq} 2jk\cos\theta\, P(\theta)\frac{e^{-jkr}}{r} \qquad (17)$$

which identifies $P(\theta)$ as the vertical radiation pattern of the source, i.e.

$E_\theta(r,\theta) \underset{r\to\infty}{}$ is proportional to $P(\theta)$. Similarly, it may be shown from Equation (16) that

$$\eta_0 H_\phi(r,\theta) \underset{r\to\infty}{} = E_\theta(r,\theta)$$

so it follows that $P(\theta)$ is also the far-field radiation pattern for H_ϕ.

There is a Fourier relationship between the radiation pattern and the fields existing at the aperture ($\rho = a$); they are not so straightforward as those given for the plane-wave case in Section 2.2 because of the presence of the Hankel functions in the cylindrical field expressions. It is convenient to introduce a new variable μ defined by

$$\mu = \sin\alpha \qquad (18)$$

so that the path of integration in the α-plane becomes the real axis in the μ-plane (c.f. Equation (7), Fig. 2(b)). Equation (16), with $\rho = a$, can now be written as,

$$H_\phi(a,z) = \frac{jk^2}{\eta_0}\int_{-\infty}^{\infty} p(\mu) H^{(2)}_1(ka\sqrt{1-\mu^2})\, e^{-jkz\mu}\, d\mu \qquad (19)$$

in which $p(\mu)$ ($= P(\alpha)$) is a new pattern function; the visible region corresponds to $-1 < \mu < 1$ and the invisible region to $|\mu| > 1$. The relationship between $H_\phi(a,z)$ and $p(\mu)$ in Equation (19) can be inverted by using the Fourier transform theorem which gives,

$$p(\mu) = \frac{\eta_0}{2\pi jkH^{(2)}_1(ka\sqrt{1-\mu^2})}\int_{-\infty}^{\infty} H_\phi(a,z)\, e^{jkz\mu}\, dz \qquad (20)$$

Equations (19) and (20) are the connecting relations between the far-field pattern function $p(\mu)$ and the tangential magnetic intensity in the aperture $H_\phi(a,z)$. There is a similar pair of relations involving the tangential electric intensity in the aperture $E_z(a,z)$ which can be derived from Equation (15); these relations are,

$$E_z(a,z) = k^2\int_{-\infty}^{\infty} p(\mu)(1-\mu^2)^{1/2} H^{(2)}_0(ka\sqrt{1-\mu^2})\, e^{-jkz\mu}\, d\mu \qquad (21)$$

$$p(\mu) = \frac{(1-\mu^2)^{-1/2}}{2\pi kH^{(2)}_0(ka\sqrt{1-\mu^2})}\int_{-\infty}^{\infty} E_z(a,z)\, e^{jkz\mu}\, dz \qquad (22)$$

If the cylindrical aperture of radius a, shown in Fig. 4, is replaced by an equivalent cylindrical sheet of current with distribution density $J_z(z)$, we can use Equations (19) and (20) by writing $H_\phi(a, z) = J_z(z)$. It follows that, if $I(z)$ is the total current distribution on an axially symmetric cylinder, the equivalent tangential magnetic intensity at the surface is given by

$$H_\phi(a,z) = \frac{I(z)}{2\pi a};$$

substituting this expression into Equation (20) gives the radiation pattern function of the cylinder.

3.2. Poynting Integration

The mean power flux density out of any point (ϕ, z) in the cylindrical aperture (Fig. 4) is

$$-E_z(a,z)\overline{H_\phi(a,z)}$$

so that the total mean power P flowing outwards from the entire length of the aperture is:

$$P = -2\pi a \int_{-\infty}^{\infty} E_z(a,z)\overline{H_\phi(a,z)}\, dz$$

Substituting the expressions for E_z and H_ϕ from Equations (19) and (21) and applying the convolution theorem (c.f. Section 2.3) we obtain an integral expression for P in terms of the pattern function $p(\mu)$, viz

$$P = \frac{4\pi^2 jk^3 a}{\eta_0} \int_{-\infty}^{\infty} |p(\mu)|^2 \frac{H_0^{(2)}(ka\sqrt{1-\mu^2})\overline{H_1^{(2)}(ka\sqrt{1-\mu^2})}}{(1-\mu^2)^{-1/2}}\, d\mu \tag{23}$$

As a result of the contour of integration, the terms $(1-\mu^2)^{1/2}$ in Equation (23) must be taken as

$$-j(\mu^2-1)^{1/2}$$

in the invisible region.

Finally, we can replace $p(\mu)$ in Equation (23) by the expression given in Equation (20) and obtain,

$$P = \frac{\eta_0 k}{4\pi^2 a} \int_{-\infty}^{\infty} |F(\mu)|^2 \frac{j(1-\mu^2)^{1/2} H_0^{(2)}(ka\sqrt{1-\mu^2})}{H_1^{(2)}(ka\sqrt{1-\mu^2})}\, d\mu \tag{24}$$

where $F(\mu)$ is the Fourier transform of the total current distribution $I(z)$ along the equivalent cylindrical aerial, i.e.

$$F(\mu) = \int_{-\infty}^{\infty} I(z) e^{jkz\mu}\, dz \tag{25}$$

Equations (24) and (25) enable us to calculate the total power P radiated by a cylindrical aerial from its far-field radiation pattern; the weighted power pattern is integrated over the range of visible $(-1 < \mu < 1)$ and invisible $(|\mu| > 1)$ angles. The resistive (radiated) power is given by $\mathrm{Re}(P)$ and the reactive power by $\mathrm{Im}(P)$. In the visible region, both Hankel function expressions in Equation (24) are complex so that this region contains both radiated and reactive powers; in the invisible region, the zero-order Hankel function is imaginary but the first-order Hankel function is real so that this region contains only reactive power. This differs from the plane-wave case in which reactive power is determined by performing the integration over the invisible region only.

Equations (24) and (25) provide the basis for determining the total impedance of a cylindrical aerial of arbitrary length $2l$, radius a, and current distribution $I(z)$, provided that the integration can be performed.

3.3. Thin-Cylinder Approximation

If the radius a of the cylindrical aperture, and hence also of the equivalent cylindrical aerial, is assumed to be small, it is found that the integral in Equation (24) becomes more manageable. To show this we write the $H_0^{(2)}$ and $H_1^{(2)}$ functions in Equation (24) as first order approximations for small (complex) arguments, i.e.

$$H_0^{(2)}(u) \underset{u\to 0}{\simeq} 1 - j\frac{2}{\pi}\log\left(\frac{\gamma u}{2}\right)$$

and

$$H_1^{(2)}(u) \underset{u\to 0}{\simeq} j\frac{2}{\pi u}$$

where u is identical to $ka(1-\mu^2)^{1/2}$ in the visible region and $-jka(\mu^2-1)^{1/2}$ in the invisible region and $\log \gamma (= 0{\cdot}5772\ldots)$ is Euler's constant. This step requires some justification; the visible and invisible parts of the integral must be considered separately.

In the visible region, u is real with a maximum value ka at $\mu = 0$. If $ka = 0{\cdot}3$, the above approximations give maximum errors of approximately $(2+j4)\%$ in $H_0^{(2)}(u)$ and -10% in $H_1^{(2)}(u)$ | with

$$|Y_1(u)| > 10J_1(u).$$

In this region therefore, it is reasonable to assume that the approximations are valid for $ka \leqslant 0{\cdot}3$. It follows that for cylinder radii $a \leqslant 0{\cdot}05\lambda$, approximate integration of Equation (24) will yield sufficiently accurate results for the radiated power and also for that part of the reactive power which resides in the visible region.

In the invisible region u becomes negative imaginary. Writing $u = -jv$, the value of u ranges from zero up through large values, where $v \simeq ka\mu$ with $\mu >> 1$, to infinity. The above Hankel function approximations for small arguments now become,

$$H_{0}^{(2)}(-jv) \underset{v\to 0}{\simeq} -j\frac{2}{\pi}\log\left(\frac{\gamma v}{2}\right)$$

and

$$H_{1}^{(2)}(-jv) \underset{v\to 0}{\simeq} -\frac{2}{\pi v}$$

In this case, $v = ka$ for $\mu = \sqrt{2}$ and if $ka = 0{\cdot}3$ the above approximations give errors of approximately $-j4\%$ and -4% in $H_0^{(2)}(u)$ and $H_1^{(2)}(u)$ respectively at the invisible angle corresponding to $\mu = \sqrt{2}$; as μ is increased above this figure, the approximations will become decreasingly accurate. However, the Hankel function expression in the integrand of Equation (24) is weighted by the factor $v|F(\mu)|^2$; it will be recalled that $F(\mu)$ is the Fourier transform of the current distribution along the cylinder. The rate at which this weighting factor falls off with increasing μ will therefore depend on the shape and extent of the current distribution $I(z)$; narrow distributions give radiation patterns which extend far into the invisible region whereas wide distributions give relatively sharp patterns. We find that with cylinders of finite (but not short) lengths carrying sinusoidal current distributions, the transform $F(\mu)$ is sufficiently sharp to validate the inclusion of the Hankel function approximations in the invisible part of the power integral for small cylinder radii. In such cases the tentative assumption* will be made that the approximate integrand will give sufficiently accurate results for total reactive power providing $a \leqslant 0{\cdot}05\lambda$.

If the above approximations are made, the real and imaginary parts of the power integral (Equation (24)) can be written as,

$$\mathrm{Re}(P) \simeq \frac{\eta_0 k^2}{8\pi}\int_{-1}^{1} |F(\mu)|^2(1-\mu^2)\,d\mu \qquad (26)$$

and

$$\mathrm{Im}(P) \simeq \frac{\eta_0 k^2}{4\pi^2}\int_{-\infty}^{\infty} |F(\mu)|^2(\mu^2-1)\left\{\frac{1}{2}\log|\mu^2-1| + \log\left(\frac{\gamma ka}{2}\right)\right\} d\mu \qquad (27)$$

* A rigorous discussion of the asymptotic behaviour of the integrand in Equation (24) is outside the scope of this report.

Equations (26) and (27) determine the resistance and reactance respectively of a thin cylinder of radius a from the Fourier transform $F(\mu)$ of its current distribution $I(z)$ (Equation (25)).

Alternatively, Equations (26) and (27) can be written in terms of the radiation pattern $P(\alpha)$. We note that the pattern function $F(\mu)(1-\mu^2)^{\frac{1}{2}}$ is proportional to $P(\alpha)$ since $\mu = \sin\alpha$. It then follows that the result for radiated power is,

$$\mathrm{Re}(P) \simeq K\int_{-\pi/2}^{\pi/2} |P(\alpha)|^2 \cos\alpha\, d\alpha$$

where K is a constant; this expression shows that Equation (26) is the conventional power integral.

It will be seen that, with the thin-cylinder approximation, the resistive power is independent of cylinder thickness whereas the reactive power depends on thickness and length through a logarithmic factor in the integrand (Equation 27).

4. REACTANCE OF A THIN DIPOLE

The extension of Poynting integration into the invisible region has been developed for the case of cylindrical apertures; we now employ the method to determine the reactance of a thin dipole with a sinusoidal current distribution along its length. The result will be compared with that obtained by two other methods.

4.1. Determination of Input Impedance

We consider a thin dipole of radius α and length $2l$ with a sinusoidal current distribution $I(z)$ as shown in Fig. 5.

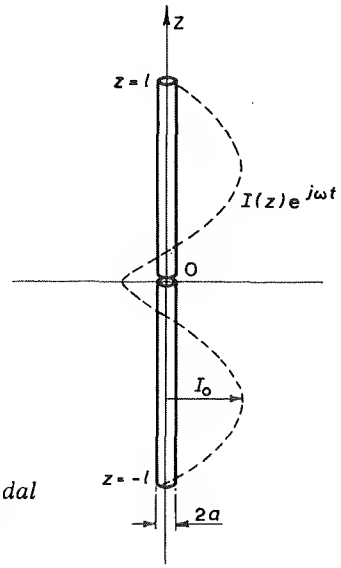

Fig. 5 - Thin dipole with sinusoidal current distribution

If we insert $I(z) = I_0 \sin k(l - |z|)$ into Equation (25) we obtain its Fourier transform $F(\mu)$, namely:

$$F(\mu) = \frac{2I_0}{k(1-\mu^2)} (\cos kl\mu - \cos kl) \qquad (28)$$

where I_0 is the loop current. The input impedance of the dipole $Z(= R + jX)$ can now be evaluated by inserting Equation (28) into Equations (26) and (27) and using the relations,

$$I_0^2 \begin{pmatrix} R \\ X \end{pmatrix} = \operatorname{cosec}^2 kl \begin{pmatrix} \mathrm{Re}(P) \\ \mathrm{Im}(P) \end{pmatrix} \qquad (29)$$

Writing $\eta_0 = 120\pi$, the expressions for R and X become:

$$R \simeq 120 \operatorname{cosec}^2 kl \int_0^1 \frac{(\cos kl\mu - \cos kl)^2}{(1-\mu^2)} d\mu \qquad (30)$$

and

$$X \simeq \frac{240 \operatorname{cosec}^2 kl}{\pi} \int_0^\infty \frac{(\cos kl\mu - \cos kl)^2}{(\mu^2 - 1)} \left\{ \frac{1}{2} \log|\mu^2 - 1| + \log\left(\frac{\gamma ka}{2}\right) \right\} d\mu \qquad (31)$$

The integral in Equation (30) can be evaluated by standard methods and the result is,

$$R \simeq \frac{30}{\sin^2 kl} \{2\mathrm{Ki}(2kl) + [\mathrm{Si}(4kl) - 2\mathrm{Si}(2kl)] \sin 2kl - [\mathrm{Ki}(4kl) - 2\mathrm{Ki}(2kl)] \cos 2kl\} \qquad (32)^*$$

which is seen to be the usual expression for the radiation resistance of a filamentary dipole[7] of length $2l$; there is no dependence on the dipole radius a.

The integral in Equation (31) is more difficult because the logarithmic part (first term) cannot be reduced to a standard form; the second term integrates into $\pi/4 \log(\gamma ka/2)\sin(2kl)$ so that the result is,

$$X \simeq \frac{60}{\sin^2 kl} \left\{ \frac{2}{\pi} \int_0^\infty \frac{(\cos kl\mu - \cos kl)^2}{(\mu^2 - 1)} \log|\mu^2 - 1| d\mu + \log\left(\frac{\gamma ka}{2}\right) \sin(2kl) \right\} \qquad (33)$$

* $\mathrm{Si}(x) = \int_0^x \frac{\sin \nu}{\nu} d\nu$ and $\mathrm{Ki}(x) = \int_0^x \frac{(1 - \cos \nu)}{\nu} d\nu$

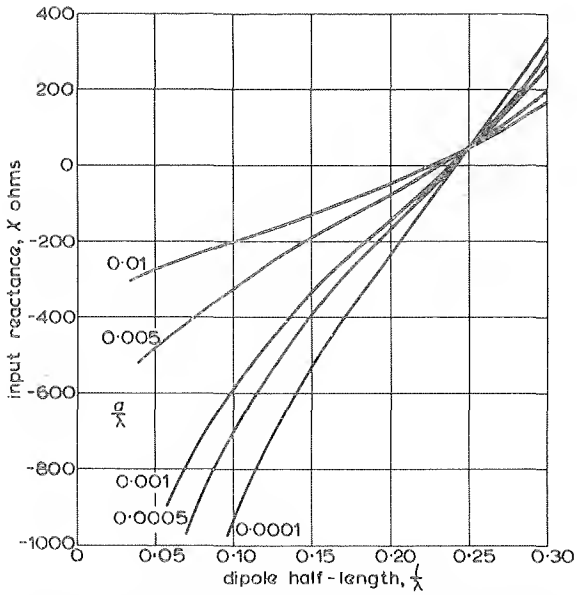

Fig. 6 - Input reactance of a thin cylindrical dipole of radius a and length 2l determined by pattern integration

which is almost the same expression as that obtained for the narrow planar dipole[1] of total width a; the two expressions differ only in that the latter result contains an additional term $-180 \cot kl$ which depends only on dipole length. For a half-wave dipole ($kl = \pi/2$) the second term in Equation (33) disappears and the reactance, as determined by numerical evaluation of the remaining integral, becomes 42·5 ohms; this is in agreement with the value of $30\mathrm{Si}(2\pi)$ obtained for a cylindrical half-wave dipole by the induced e.m.f. method.[8]

For lengths other than odd multiples of a half-wavelength the input reactance depends on the radius as well as the length of the dipole. In Fig. 6, the reactance X determined from Equation (33) is plotted as a function of dipole half-length l for varying dipole radii a/λ. The results show that the input reactance depends very largely on the dipole thickness and becomes very high for thin dipoles. The general variation is very similar to that obtained by the conventional induced e.m.f. method.

4.2. Comparison with Other Methods

It is of interest to compare the results obtained for the input reactance of a thin cylindrical dipole by pattern integration with those given by some other methods. Particularly important is the induced e.m.f. method which employs the result for the mutual impedance between two identical dipoles to determine their self-reactance.

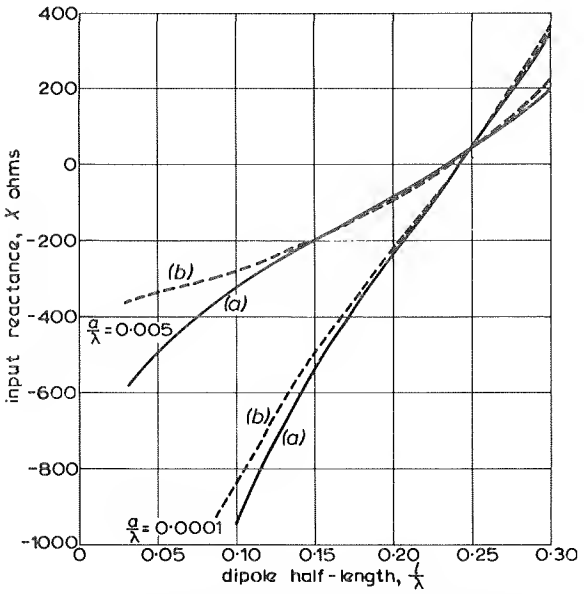

Fig. 7 - Input reactance of thin cylindrical dipole - comparison of results obtained from
(*a*) pattern integration (*b*) induced e.m.f. method

In Fig. 7 we have re-plotted two of the results from Fig. 6 together with those obtained by the conventional induced e.m.f. method* for the same dipole thicknesses. It will be seen that there is little difference between these results in the region of dipole-resonance ($l/\lambda \simeq 0{\cdot}25$) but that for short dipoles the results diverge, with the present results (curves (*a*)) giving larger capacitive reactances than the induced e.m.f. method (curves (*b*)). (It will be recalled from Section 3.3 that the approximate theory (Equations (26) and (27)) is expected to give errors for short distributions.) For extremely thin dipoles, however, both solutions approximate to the expression, $X \simeq 120 \cot(kl)\log(a/\lambda)$, and the fractional difference between the results obtained by the two methods would be insignificant.

The reactance of a thin cylindrical dipole may also be estimated from that of the planar dipole by using an electrostatic transformation which can be applied to uniform systems of conductors carrying TEM waves. Assuming that a cylindrical dipole of radius a is equivalent to a strip-dipole of total width $4a$, we find from Reference 1 that the new expression for input reactance differs from that given in Equation (33) by an additional capacitive reactance of approximately $14\cot kl$. This means that the difference between the two results is insignificant over the range of interest (i.e. near dipole-resonance) with the results diverging for very short dipoles; the latter effect is not surprising because the above transformation takes no account of end effects and the approximate power integration becomes inaccurate for short distributions.

* The induced field is evaluated over a cylindrical surface of radius $\sqrt{2}a$ (see Reference 8).

5. CONCLUSIONS

It has been shown that it is possible to determine the reactance of a cylindrical dipole from its far-field radiation pattern by suitably integrating the power pattern over the visible and invisible angular regions; this has extended to cylindrical systems the new principle of analytic continuation of the Poynting vector method recently described for planar radiators.

For thin dipoles, the Poynting integrand reduces to a manageable expression and the reactance in this case has been evaluated for several dipole sizes and compared with that obtained using the well-known induced e.m.f. method. The conclusion is that the difference between the results of the two methods is insignificant over a large range of dipole sizes near the first resonance; the agreement is exact for the thin half-wave dipole and is independent of thickness.

It is emphasized that the new method is not restricted to thin dipoles; the only difficulty in applying it to thick dipoles with arbitrary current distributions is actually evaluating the complex integral expressions for reactance which obtain in such cases.

Finally, it should be pointed out that the new method, which involves complex power integration over the aerial surface, actually uses an induced e.m.f. technique; the essential difference between the new and the conventional methods is that in the former, mathematical manipulation allows the power integral to be stated in terms of the far-field radiation pattern of the aerial rather than its near-field expressions.

6. REFERENCES

1. RHODES, D.R. 1964. On a fundamental principle in the theory of planar antennas. *Proc. I.E.E.E.*, 1964, **52**, 9, pp. 1013 - 21.

2. WOODWARD, P.M. *and* LAWSON, J.D. 1948. The theoretical precision with which an arbitrary radiation-pattern may be obtained from a source of finite size. *J.Instn elect.Engrs.*, September 1948, **95**, III, 37, pp. 363 - 370.

3. STRATTON, J.A. 1941. Electromagnetic theory. New York, McGraw-Hill Book Co. Inc., 1941, pp. 361 - 364.

4. ERDELYI, A. 1965. Asymptotic expansions. New York, Dover, 1965, p. 51.

5. BRACEWELL, R. 1965. The Fourier transform and its applications. New York, McGraw-Hill, 1965, pp. 108 - 115.

6. STRATTON, J.A., *loc.cit.*, pp. 349 - 356.

7. JORDAN, E.C. 1953. Electromagnetic waves and radiating systems. London, Constable, 1953, p. 345.

8. *Ibid*, pp. 359 - 363.

7. APPENDIX

Collapse of Triple Power Integral into Single Form

The triple integral to be considered is

$$I = \int_{-\infty}^{\infty} \left(\int_{-\infty}^{\infty} f_1(\psi) e^{-jky\psi} d\psi \right) \left(\int_{-\infty}^{\infty} \overline{f_2(\psi)} e^{jky\psi} d\psi \right) dy \quad (34)$$

where, from Section 2.3, we have

$$f_1(\psi) = (1-\psi^2)^{-\frac{1}{2}} p(\psi) \text{ and } f_2(\psi) = p(\psi)$$

Equation (34) in its simplest form is written as:

$$I = \int_{-\infty}^{\infty} Tf_1(\psi) \overline{Tf_2(\psi)} dy \quad (35)$$

when T is an operator denoting "the Fourier transform of". The convolution theorem is now applied; in its usual form it can be written,

$$T \int_{-\infty}^{\infty} f_1(\psi) f_2(x-\psi)\, d\psi = Tf_1(\psi)\, Tf_2(\psi)$$

so that we have*

$$T \int_{\infty}^{\infty} f_1(\psi) \overline{f_2(\psi - x)}\, d\psi = Tf_1(\psi)\, \overline{Tf_2(\psi)}$$

* If $Tf(\psi) = F(s)$ and $\overline{Tf(\psi)} = G(s)$, then $\overline{F(s)} = G(-s)$.

It therefore follows that

$$\int_{-\infty}^{\infty} f_1(\psi) \overline{f_2(\psi - x)}\, d\psi = T^{-1} \left\{ Tf_1(\psi) \overline{Tf_2(\psi)} \right\} \quad (36)$$

The r.h.s. of Equation (36) is the integral:

$$\frac{1}{2\pi} \int_{-\infty}^{\infty} Tf_1(\psi) Tf_2(\psi) e^{jkyx}\, d(ky)$$

If we now set $x = 0$, Equations (35) and (36) give

$$\frac{kI}{2\pi} = \int_{-\infty}^{\infty} f_1(\psi) f_2(\psi) d\psi$$

so that we have,

$$I = \frac{2\pi}{k} \int_{-\infty}^{\infty} f_1(\psi) \overline{f_2(\psi)}\, d\psi \quad (37)$$

Equation (37) is the single integral equivalent of Equation (34) and is the required result. This form of the power integral has been used in deriving Equation (12), Section 2.3, and Equation (23) Section 3.2 in the main text.

JMP

Printed by BBC Research Department, Kingswood Warren, Tadworth, Surrey